

# Synthesis and Characterization of the Crystal and Magnetic Structure and Properties of the Hydroxyfluorides Fe(OH)F and Co(OH)F

Hamdi Ben Yahia<sup>a,\*</sup>, Masahiro Shikano<sup>a,\*</sup>, Mitsuharu Tabuchi<sup>a</sup>, Hironori Kobayashi<sup>a</sup>, Maxim Avdeev<sup>b</sup>, Thiam Teck Tan<sup>c</sup>, Samuel Liu<sup>d</sup>, Chris D. Ling<sup>d</sup>,

<sup>a</sup> *Research Institute for Ubiquitous Energy Devices, National Institute of Advanced Industrial Science and Technology (AIST), 1-8-31, Midorigaoka, Ikeda, Osaka 563-8577, Japan. Fax: +81-72-751-9609; Tel: +81-72-751-7932; E-mail: benyahia.hamdi@voila.fr, shikano.masahiro@aist.go.jp.*

<sup>b</sup> *Bragg Institute, B87, Australian Nuclear Science and Technology Organisation, Locked Bag 2001 Kirrawee DC NSW 2232, Australia.*

<sup>c</sup> *School of Materials Science and Engineering, University of New South Wales, NSW 2052, Australia*

<sup>d</sup> *School of Chemistry, The University of Sydney, Sydney, NSW 2006, Australia.*

<sup>†</sup> Electronic Supplementary Information (ESI) available:

---

## Abstract

The title compounds were synthesized by a hydrothermal route from a 1:1 molar ratio of lithium fluoride and transition metal acetate in an excess of water. The crystal structures were determined using a combination of powder and/or single crystal X-ray and neutron powder diffraction measurements. The magnetic structure and properties of Co(OH)F were characterized by magnetic susceptibility and low-temperature neutron powder diffraction measurements.  $M(\text{OH})\text{F}$  ( $M = \text{Fe}, \text{Co}$ ) crystallizes with structures related to diaspore-type  $\alpha\text{-AlOOH}$ , with the  $Pnma$  space group,  $Z = 4$ ,  $a = 10.471(3) \text{ \AA}$ ,  $b = 3.2059(10) \text{ \AA}$ , and  $c = 4.6977(14) \text{ \AA}$ , and  $a = 10.2753(3) \text{ \AA}$ ,  $b = 3.11813(7) \text{ \AA}$ , and  $c = 4.68437(14) \text{ \AA}$ , for Fe- and Co-phases, respectively. The structures consist of double chains of edge-sharing  $M(\text{F},\text{O})_6$  octahedra running along the  $b$ -axis. These infinite chains share corners and give rise to channels. The protons are located in the channels and form O-H...F *bent* hydrogen bonds. The magnetic susceptibility indicates an antiferromagnetic ordering at  $\sim 40$  K and the neutron powder diffraction measurements at 3 K show that the ferromagnetic rutile-type chains with spins parallel to the short  $b$ -axis are antiferromagnetically coupled to each other, similarly to the magnetic structure of goethite  $\alpha\text{-FeOOH}$ .

**Keywords:** Single crystal structure, Hydrogen bond, Powder neutron diffraction, Magnetic structure, Electrode materials, Lithium battery.

## 1. Introduction

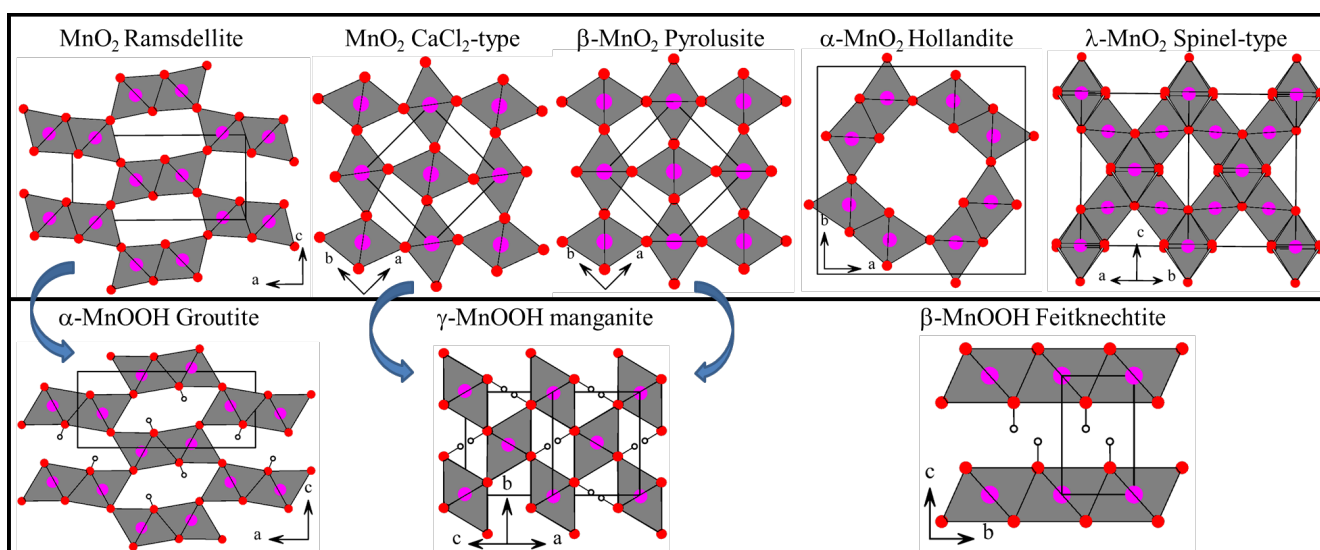


**Figure 1.** The structural relationship between the MnO<sub>2</sub> and MnOOH polymorphs.

The manganese dioxides MnO<sub>2</sub> are well known to exhibit several structural forms. Among them, the mineralogical β-MnO<sub>2</sub> (pyrolusite  $P4_2/mnm$ ,  $a = 4.388$ ,  $c = 2.865$  Å) and MnO<sub>2</sub> (ramsdellite  $Pnma$ ,  $a = 9.2734$ ,  $b = 2.8638$ ,  $c = 4.5219$  Å) are the most stable.<sup>1,2</sup> These forms are isostructural to rutile TiO<sub>2</sub> and diaspore α-AlOOH structures, respectively.<sup>3,4</sup> At relatively low pressure (0.3 GPa) a second-order phase transition occurs from β-MnO<sub>2</sub> to CaCl<sub>2</sub>-type-MnO<sub>2</sub> form (CaCl<sub>2</sub>-type,  $Pnnm$ ,  $a = 4.312$ ,  $b = 4.437$ ,  $c = 2.862$  Å) which crystallizes with a distorted rutile structure.<sup>5</sup> At 46 GPa, CaCl<sub>2</sub>-type-MnO<sub>2</sub> transforms to a cubic phase ( $a = 4.484$  Å) similar to SiO<sub>2</sub> ( $Pa-3$  or  $Fm-3m$ ).<sup>5</sup> A few other MnO<sub>2</sub> synthetic forms have also been prepared, such as α-MnO<sub>2</sub> (Hollandite  $I4/m$ ,  $a = 9.7876$ ,  $c = 2.865$  Å) or λ-MnO<sub>2</sub> (spinel  $Fd-3m$ ,  $a = 8.03$  Å), obtained by precipitation method and electrochemical lithium deintercalation from the spinel-LiMn<sub>2</sub>O<sub>4</sub> phase (spinel  $Fd-3m$ ,  $a = 8.24$  Å), respectively.<sup>6,7</sup>

In pyrolusite, CaCl<sub>2</sub>-type, and ramsdellite, hexagonal close-packed arrays of oxygen atoms are observed; whereas the spinel has cubic close-packed oxygen arrays. In all these compounds, the manganese atoms are octahedrally coordinated. However, since the connectivity between these polyhedra is different, one- to three-dimensional empty channels have been observed (Figure 1). This structural feature has attracted considerable attention from electrochemists.<sup>8-10</sup> and ref. therein Indeed, since

there is a need for high-performance electrode materials for high-power lithium-ion batteries (LIBs), several researchers have attempted to replace the graphite anode employed in practical electrodes (theoretical specific capacity of 372 mAh g<sup>-1</sup>) by manganese dioxides (theoretical capacity of 1,232 mAh g<sup>-1</sup>). Furthermore, MnO<sub>2</sub> is intensively used in primary alkaline cells. The key reaction of MnO<sub>2</sub> in these cells is:  $\text{MnO}_2 + \text{e}^- + \text{H}^+ \rightarrow \text{MnOOH}$ .<sup>11</sup> These manganese oxyhydroxides MnOOH also exist in several modifications: the minerals  $\alpha$ -MnOOH (groutite, *Pnma*,  $a = 10.667$ ,  $b = 2.871$ ,  $c = 4.554 \text{ \AA}$ ) with the diaspore  $\alpha$ -AlOOH structure;  $\beta$ -MnOOH (feitknechtite, *P-3m*,  $a = 3.32 \text{ \AA}$ ,  $c = 4.71 \text{ \AA}$ ) isotypic with pyrochroite Mn(OH)<sub>2</sub>; and  $\gamma$ -MnOOH (manganite, *P2<sub>1</sub>/c*,  $a = 5.304$ ,  $b = 5.277 \text{ \AA}$ ,  $c = 5.304 \text{ \AA}$ ,  $\beta = 114.38^\circ$ ) with a modified rutile-type structure (Figure 1).<sup>12-14</sup> Synthetic MnOOH is the simplest and most practical precursors for the preparation of manganese oxides, intercalation compounds and lithium manganese oxides for LIBs. When the trivalent manganese ion is replaced by a divalent transition metal or alkali earth metal ion, and one oxide ion is replaced by a fluoride ion, a homologous family of compounds is formed. The *M(OH)F* ( $M = \text{Mg, Co, Ni, Cu, Zn, Cd, and Hg}$ ) compounds do indeed exist and their crystal structures are strongly related to the  $\alpha$ -,  $\beta$ -, and  $\gamma$ -MnOOH polymorphs.<sup>15-23</sup> Recently, during our attempts to synthesize the LiMOF ( $M = \text{Mn, Fe, and Co}$ ) compositions, we obtained new *M(OH)F* compounds. The Fe(OH)F and Co(OH)F structures are related to the diaspore  $\alpha$ -AlOOH structure, whereas Mn(OH)F crystallizes with a distorted rutile structure related to CaCl<sub>2</sub>-type.

In the present work we report that we have synthesized the new compounds *M(OH)F* ( $M = \text{Fe and Co}$ ) and solved their crystal structures using the combination of powder and/or single crystal X-ray and neutron powder diffraction measurements. We have also characterized the Co(OH)F magnetic structure and properties by neutron powder diffraction (NPD) and magnetic susceptibility measurements.

## 2. Experimental Section

### 2.1. Synthesis

Fe(OH)F and Co(OH)F were obtained by hydrothermal synthesis from a 1:1 molar ratio of lithium fluoride and transition metal acetates. Each starting material was separately dissolved in 30 mL of distilled water, preheated at 50 °C. The two solutions were then mixed and left stirring for one hour. The solutions were finally poured into 100 mL autoclaves, which were sealed in a glove box under an argon or nitrogen atmosphere and heated at 200 °C for 48 h. By filtering the solutions, dark green and pink-colored powders were obtained for Fe- and Co-phases, respectively. An attempt to prepare Ni(OH)F under the same conditions led to Ni(OH)<sub>2</sub>. It is worth pointing out that the amount of Co(OH)F powder obtained was much larger than of Fe(OH)F, although the same preparation process was used.

The Fe(OH)F single crystals used for the data collection were obtained from a 3:1 mixture of iron oxalate and lithium fluoride which was fired at 200 °C for 60 h then cooled slowly to room temperature at a rate of 15 °C h<sup>-1</sup>. For Co(OH)F, no single crystals could be obtained even after a long treatment (two weeks at 200 °C). Most of the Fe(OH)F single crystals were relatively large twinned needles, while the Co(OH)F powder consisted mostly of nano-fibers (Figure 2).

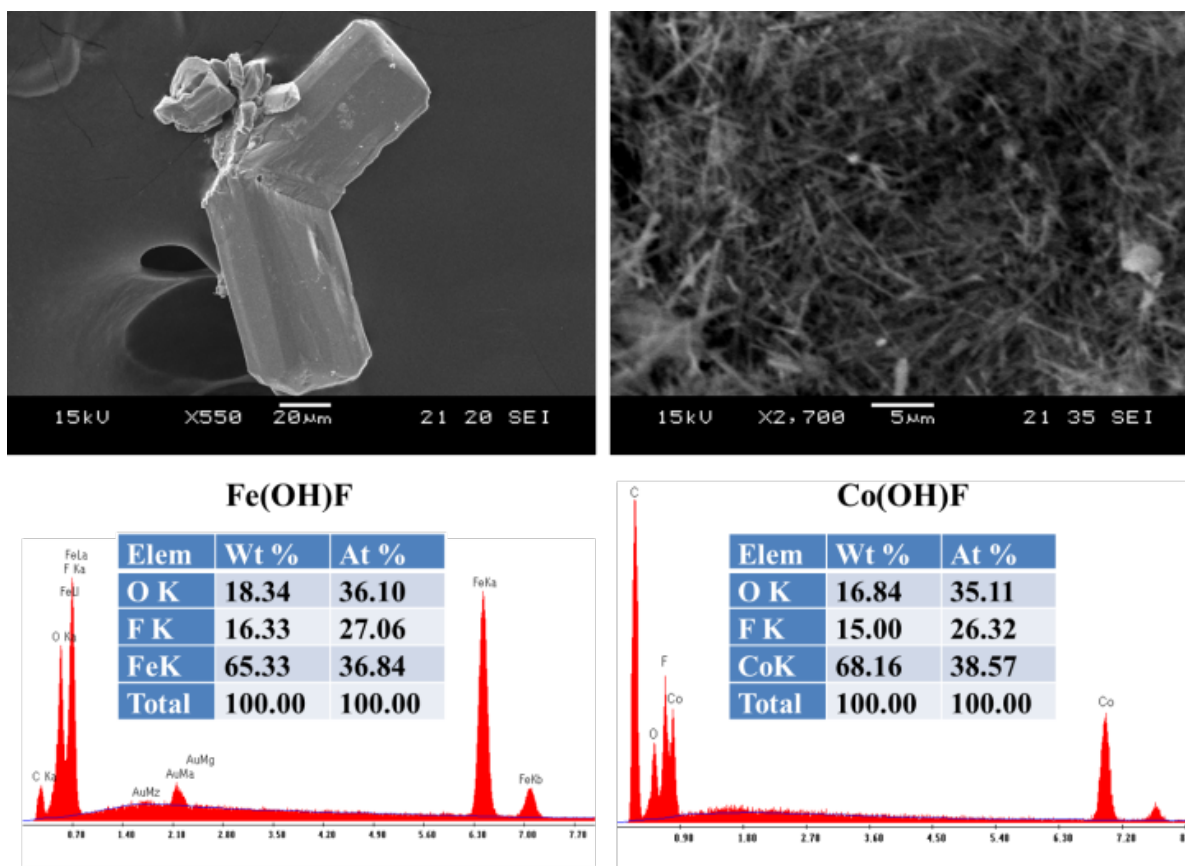


**Figure 2.** SEM images of Fe(OH)F twinned single crystals and Co(OH)F nano-fibers.

## 2.2. Electron microprobe analysis

Semi-quantitative energy-dispersive X-ray (EDX) analyses of the  $M(\text{OH})\text{F}$  powders and single crystals, including the ones investigated on the diffractometer, were carried out with an EDAX Genesis analyzer installed JSM-5500LV (JEOL) scanning electron microscope (SEM). The experimentally observed compositions were close to the ideal  $M(\text{OH})\text{F}$  (Figure 2 and S1).<sup>†</sup> The Fe(OH)F powder contained a large amount of  $\text{Fe}_3\text{O}_4$ .

## 2.3. X-Ray diffraction

To ensure the purity of  $M(\text{OH})\text{F}$  powders, routine powder XRD measurements were performed. Data were collected at room temperature over the  $2\theta$  range  $5 \leq 2\theta \leq 80^\circ$  with a step size of  $0.01^\circ$  on a RINT-TTR diffractometer (Rigaku) with monochromated  $\text{CuK}\alpha$  radiation. Full pattern-matching

refinements were performed with the Jana2006 program package.<sup>24</sup> The background was estimated by a Legendre function, and the peak shapes were described by a pseudo-Voigt function. This revealed the presence of a large amount of Fe<sub>3</sub>O<sub>4</sub> (45 Wt %) in the samples prepared under argon and nitrogen (Figure 3). High resolution powder XRD using synchrotron radiation ( $\lambda = 0.5001 \text{ \AA}$ ) were also collected on BL19B2 at SPring-8 [with the approval of the Japan Synchrotron Radiation Research Institute (Proposal No. 2012B1598)] for Co(OH)F (Figure S2).<sup>†</sup> Evaluation of these data yielded the refined cell parameters  $a = 10.29935(14)$ ,  $b = 3.12808(4)$ ,  $c = 4.69171(8) \text{ \AA}$ , and  $V = 151.154(5) \text{ \AA}^3$ .

Single crystals of Fe(OH)F suitable for XRD were selected on the basis of the size and the sharpness of the diffraction spots. The data collection was carried out on a Smart Apex diffractometer using MoK $\alpha$  radiation. Data processing and all refinements were performed with the JANA2006 program.<sup>24</sup> A Gaussian-type absorption correction was applied and the shape was determined with the video microscope. For data collection details, see Table 1.

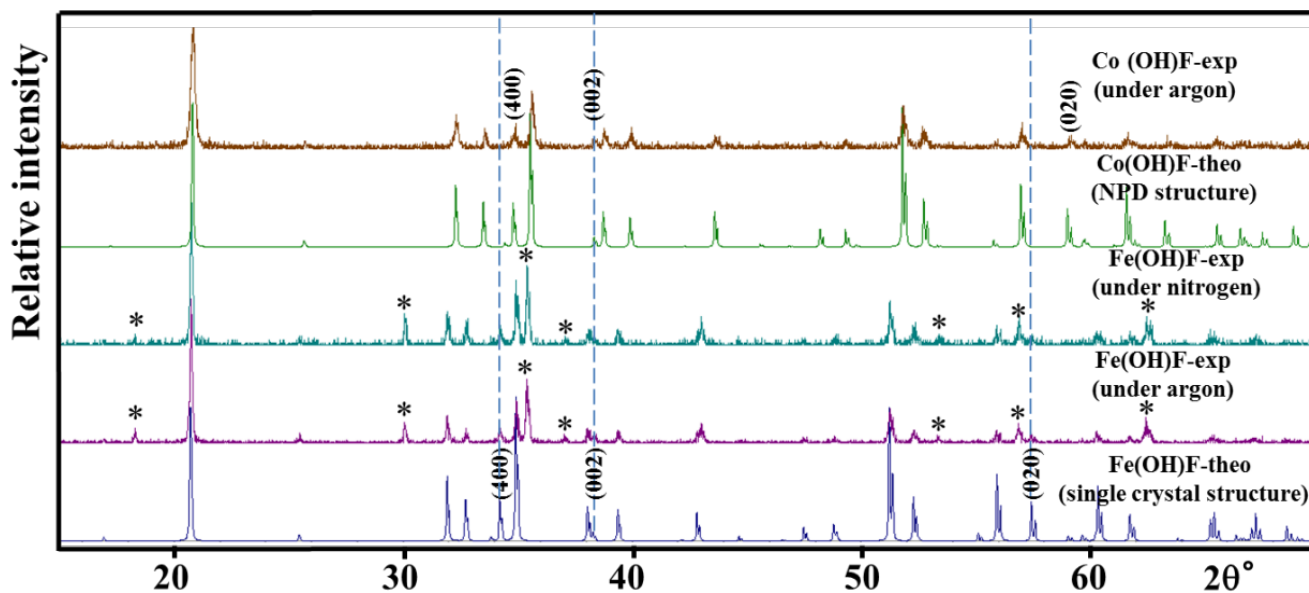


**Figure 3.** Powder XRD patterns of Fe(OH)F and Co(OH)F, obtained from hydrothermal syntheses.

<sup>15</sup> The asterisk correspond to Fe<sub>3</sub>O<sub>4</sub> ( $Fd-3m$ ,  $a = 8.408 \text{ \AA}$ ).<sup>25</sup>

**Table 1.** Crystallographic data and structure refinement details for Fe(OH)F.

Formula	Fe(OH)F
Crystal color	Green-yellow
Crystal size	0.120× 0.055× 0.028
$M$ , g mol <sup>-1</sup>	91.85
Crystal system	orthorhombic
Space group	<i>Pnma</i>
$a$ , Å	10.471 (3)
$b$ , Å	3.2059 (10)
$c$ , Å	4.6977 (14)
$V$ , Å <sup>3</sup>	157.70 (8)
$Z$	4
Density calcd., g cm <sup>-3</sup>	3.87
Temperature, K	293 (1)
$F(000)$ , e	176
Diffractometer	Smart Apex
Monochromator	Graphite
Radiation	MoK $\alpha$ , 0.71069 Å
Scan mode	Multi-scan
$hkl$ range	-9 < $h$ < 13 -4 < $k$ < 3 -6 < $l$ < 5
$\theta_{\min}$ , $\theta_{\max}$ , deg	3.89, 27.75
Linear absorption coeff., mm <sup>-1</sup>	9.067
Absorption correction	Gaussian
$T_{\min}/T_{\max}$	0.647
No. of reflections	801
No. of independent reflections	212
Reflections used	202
$R_{\text{int}}$	0.023
Refinement	$F^2$
No. of refined parameters	20
$R$ factors $R(F)$ / $wR(F^2)$	0.0211 / 0.0519
g. o. f.	1.14
Weighting scheme	$w = 1/(\sigma^2(I) + 0.0009I^2)$
Diff. Fourier residues, e <sup>-</sup> Å <sup>-3</sup>	-0.27/ +0.24

## 2.4. Magnetic susceptibility measurements

Magnetic susceptibility measurements of Co(OH)F were carried out using a Quantum Design Physical Properties Measurement System (PPMS) with a vibrating sample magnetometer (VSM) probe. The susceptibility was recorded in the zero field-cooled (ZFC) and 5 kOe field-cooled (FC) modes over the temperature range 2–300 K. Magnetization data as a function of field were collected up to  $\pm 50$  kOe at 5 K after cooling the sample under a field of 50 kOe.

## 2.5. Neutron powder diffraction

Neutron powder diffraction (NPD) data were collected on the high-resolution diffractometer



Echidna at the OPAL facility (Lucas Height, Australia) using neutrons of wavelength 1.6215 Å. For the measurements, the sample in the form of ~1 g of powder was loaded in a 6 mm diameter cylindrical vanadium can and data collected at 75 and 3 K, *i.e.*, above and below the magnetic transition, using a closed-cycle refrigerator. Rietveld analysis of the data was performed using the Fullprof Suite with the default neutron scattering lengths and Co<sup>2+</sup> magnetic form-factor.<sup>26</sup>

### 3. RESULTS AND DISCUSSION

#### 3.1. Structure refinement

##### 3.1.1. *Fe(OH)F* structure refinement from single crystal data

The extinction conditions observed for Fe(OH)F were compatible with the space groups *Pnma* (centrosymmetric) and *Pna2<sub>1</sub>* (non-centrosymmetric). The structure was solved in the space group *Pnma*. The three atomic positions forming the octahedral units were located using the superflip program implemented in Jana2006. At this stage the chemical formula (FeO<sub>2</sub>) was in contradiction with the EDX analysis, which shows the presence of Fe/F/O mixture. Therefore, a F/O statistical disorder was introduced and constraints on the anisotropic atomic displacement parameters (ADPs) and occupancies have been set [ $\text{Occ}(\text{O}) = 1 - \text{Occ}(\text{F})$  and  $\text{ADP}(\text{O}) = \text{ADP}(\text{F})$ ]. The refinement then yields the chemical formula FeF<sub>2-x</sub>O<sub>x</sub> and the structure is isotopic to the ramsdellite MnO<sub>2</sub> structure.<sup>2</sup> Since the iron ions are expected to be divalent, we suspected the presence either of *x*Li or *x*H in order to compensate for the excess of negative charges. The use of difference-Fourier syntheses allowed us to localize the remaining proton positions on 4*c* sites with distances around ~0.85 Å from the O sites. By introducing these positions and setting new constraints [ $\text{Occ}(\text{H}) = \text{Occ}(\text{O}) = 1 - \text{Occ}(\text{F})$  and  $\text{ADP}(\text{H}) = \text{ADP}(\text{O}) = \text{ADP}(\text{F})$ ], the occupancies converged to values close to 0.5 but large fluctuation of H1 was observed. Therefore, in the final refinement, the H1 position and the occupancies (0.5 for all

atoms) were fixed. This led to the residual factors listed in Table 1. The refined atomic positions and (ADPs) are given in Table 2. Further details on the structure refinement may be obtained from the Fachinformationszentrum Karlsruhe, D-76344 Eggenstein-Leopoldshafen (Germany), by quoting the Registry No. CSD-425870.

5

**Table 2.** Atom positions, equivalent isotropic and anisotropic ADPs for Fe(OH)F. The anisotropic ADP factor exponent takes the form:  $-2\pi^2[(ha^*)^2U_{11}+\dots+2hka^*b^*U_{12}]$ .

Atom	Wyck.	Occ.	x	y	z	$U_{eq} (\text{\AA}^2)$
Fe1	4c	1	0.36438(4)	1/4	0.47205(11)	0.0141(2)
F1	4c	0.5	0.5567(10)	1/4	0.302(2)	0.0156(7) *
O1	4c	0.5	0.5478(13)	1/4	0.284(3)	0.0156(7) *
H1	4c	0.5	0.59718	1/4	0.14741	0.0156(7) *
F2	4c	0.5	0.2988(7)	3/4	0.2200(17)	0.0149(7) *
O2	4c	0.5	0.3119(9)	3/4	0.194(2)	0.0149(7) *
H2	4c	0.5	0.622(7)	1/4	0.912(18)	0.0149(7) *
Atom	$U_{11}$	$U_{22}$	$U_{33}$	$U_{12}$	$U_{13}$	$U_{23}$
Fe1	0.0124(4)	0.0121(4)	0.0176(4)	0.00000	-0.00034(16)	0.00000

\*:  $U_{iso}$

**Table 3.** Crystal structural parameters for  $\text{Co(OH)}_{0.86(3)}\text{F}_{1.14(3)}$  based on the Rietveld refinement against  
 10 NPD data collected at 75 K. Space group  $Pnma$  (No 62),  $a = 10.2753(3)$ ,  $b = 3.11813(7)$ ,  $c = 4.68437(14)$  \AA,  $V = 150.09(1)$  \AA<sup>3</sup>.

Atom	Wyck.	Occ.	x	y	z	$B_{iso}, \text{\AA}^2$
Co	4c	1	0.3668(10)	1/4	0.4751(17)	0.94(10)
F1/O1	4c	0.658/0.342(10)	0.5521(4)	1/4	0.2938(9)	0.62(8)
H1	4c	=Occ.(O1)	0.5723(14)	1/4	0.088(3)	= $B_{iso}$ (F1/O1)
F2/O2	4c	0.476/0.524(12)	0.3049(4)	3/4	0.2097(9)	0.72(7)
H2	4c	=Occ.(O2)	0.6278(12)	1/4	0.9514(18)	= $B_{iso}$ (F2/O2)

### 3.1.2. Co(OH)F structure refinement from neutron powder diffraction data

The average Mg(OH)F crystal structure was used as starting model for Rietveld refinement against Co(OH)F NPD data.<sup>15</sup> Initially, the protons were introduced in the structure as hydroxyl groups fully ordered with fluorine; however, difference Fourier maps clearly showed extra nuclear density located at  $\sim 1$  Å from the nominally fluorine position that strongly suggested partial (O,F) disorder. This was further supported by an improved agreement between the calculated and observed diffraction patterns after allowing partial F/OH disorder: the  $R_p$ ,  $R_{wp}$ ,  $R_{Bragg}$ , and  $\chi^2$  were reduced from 1.77%, 2.42%, 12.0%, and 3.69 to 1.20%, 1.49%, 6.81%, and 1.41 respectively. Therefore, the model with partial F/OH disorder similar to that previously reported for ZnOHF,<sup>19</sup> was used for further analysis of the NPD data. Since O and F atoms have very close neutron scattering lengths ( $b_c = 5.830$  and  $5.654$  fm, respectively), the  $x$  value in  $\text{Co(OH)}_x\text{F}_{2-x}$  could not be determined from the refinement of the atomic occupancies for the common (O,F) site. However, as hydrogen is a relatively strong neutron scatterer ( $b_c = -3.74$  fm) the refinement using constraints  $\text{occ(H)}=\text{occ(O)}=1-\text{occ(F)}$  for two inequivalent sites could be used to determine  $x$  quite precisely, resulting in the composition  $\text{Co(OH)}_{0.86(3)}\text{F}_{1.14(3)}$ . The final Rietveld plot and crystallographic information for  $\text{Co(OH)}_{0.86(3)}\text{F}_{1.14(3)}$  at 300 and 75 K, *i.e.*, in the paramagnetic state, are presented in Figure 4 and Table 3.

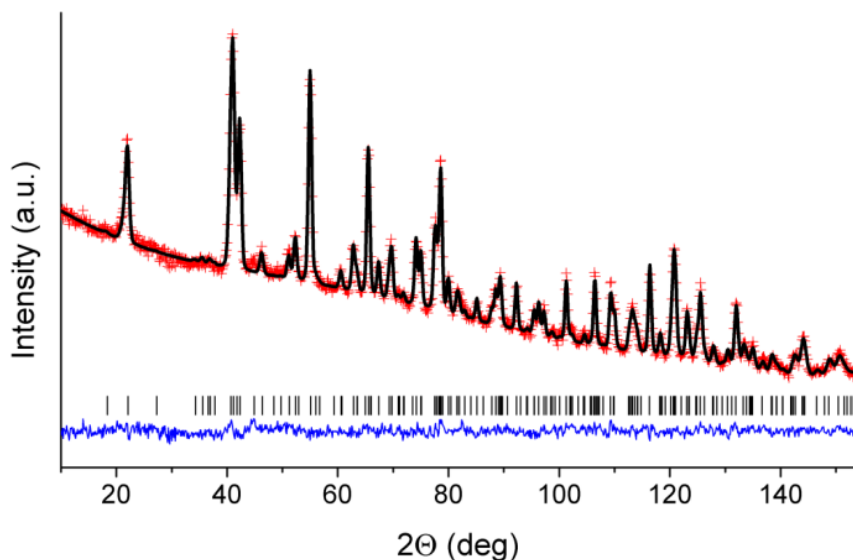


**Figure 4.** The Rietveld plot for  $\text{Co(OH)}_{0.86(3)}\text{F}_{1.14(3)}$  for the NPD data collected at 75 K,  $R_p = 1.20\%$ ,  $R_{wp} = 1.49\%$ ,  $R_{Bragg} = 6.81\%$ ,  $\chi^2 = 1.41$ .

### 3.2. Crystal structure

A projection view of the structure of Fe(OH)F, a derivative of the  $\alpha$ -AlOOH diaspore structure, is displayed in Figure 5a with the oxygen polyhedra drawn around the transition metals. The Fe(OH)F structure consists of double chains of edge-sharing Fe(F,O)<sub>6</sub> octahedra running along the *b*-axis (Figure 5b). These infinite chains share corners and give rise to tunnels in which the protons are located. Interatomic distances and bond valence sums (BVSs)<sup>27, 28</sup> are listed in Table 4.

The Fe(F,O)<sub>6</sub> octahedra are distorted with F,O statistical disorder. The Fe–O distances range from 2.115 to 2.175 Å with an average value of 2.144 Å, whereas the Fe–F distances range from 2.068 to 2.167 Å with an average value of 2.106 Å. This leads to an average Fe–O,F distance of 2.125 Å. The BVS of 1.89 is in agreement with the expected value of +2 for Fe<sup>2+</sup>.

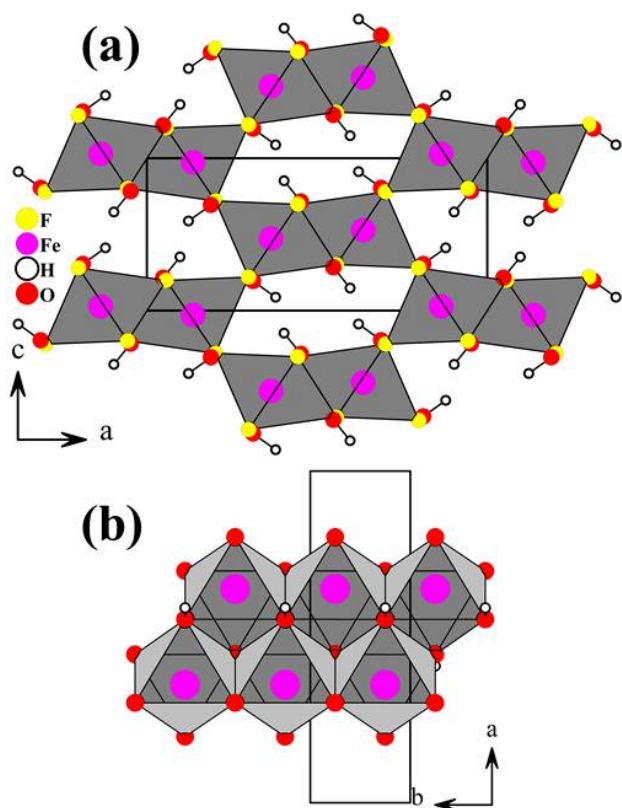


**Figure 5.** Projection views of the crystal structures of Fe(OH)F on the (010) plane, and of the double chains of edge-sharing octahedra running along the *b*-axis on the (001) plane. Thick solid blue lines emphasize the shape of the 1-D channels.

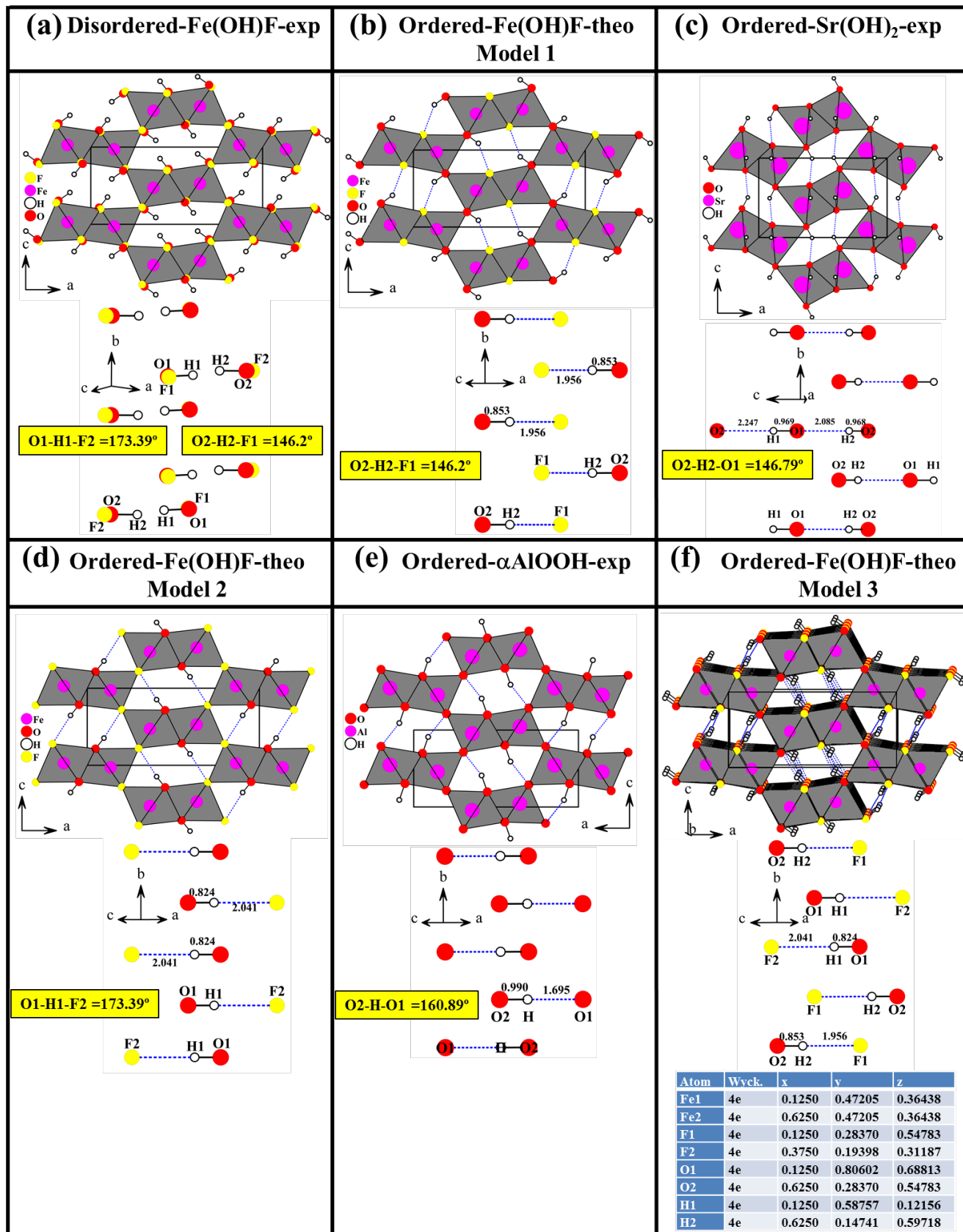
The occurrence of short H1...H2, O1...H2, and O2...H1 distances of 1.13, 1.91, and 1.865 Å, respectively may indicate serious structural problems (Alert level A in *checkcif*). However, these short distances can be well explained by the fluorine/oxygen statistical disorder. Simple distance considerations show that all the (F/OH)...(HO/F) interactions are in reality OH...F hydrogen bonds, since, opposite to each hydroxyl group there must be a fluorine atom. More details about the hydrogen bond geometries are depicted in Figure 6a, b, and d.

Table 4. Interatomic distances and bond valence sums (BVS) for Fe(OH)F and Co(OH)<sub>0.86(3)</sub>F<sub>1.14(3)</sub>.

Average distances are given in angle brackets.

	Distance (Å)	BVS
<b>Fe(OH)F-single crystal XRD at room temperature</b>		
Fe1-O1	2.115(14)	0.357
Fe1-O2	2.120(10)	0.352
Fe1-O2 (×2)	2.140(7)	0.334
Fe1-O1 (×2)	2.175(9)	0.304
	<2.144>	1.985 <sup>a</sup>
Fe1-F2	2.068(8)	0.331
Fe1-F1 (×2)	2.094(7)	0.308
Fe1-F2 (×2)	2.108(5)	0.297
Fe1-F1	2.167(11)	0.253
	<2.106>	1.794 <sup>a</sup>
		<1.889> <sup>a</sup>
F1-O1	0.125(18)	
F2-O2	0.183(13)	
O1-H1	0.823(14)	
O2-H2	0.86(7)	
F2-H1	2.041(8)	
F1-H2	1.95(8)	
H1-H2	1.13(8)	
<b>CoF<sub>2-x</sub>(OH)<sub>x</sub>NPD at 75 K</b>		
Co1-O1,F1 (×2)	2.073(7)	0.357/0.318
Co1-O2,F2	2.079(11)	0.351/0.313
Co1-O1,F1	2.085(11)	0.346/0.308
Co1-O2,F2 (×2)	2.093(6)	0.338/0.301
	<2.083>	<1.957> <sup>a</sup>
O1-H1	0.986(15)	
O2-H2	1.024(11)	
F1-H2	1.783(10)	
F2-H1	1.881(15)	
H1-H2	0.857(18)	

<sup>a</sup> bond valence sum,  $BVS = \exp\{(r_0-r)/b\}$  with the following parameters:  $b = 0.37$ ,  $r_0(\text{Fe}^{\text{II}}-\text{F}) = 1.658$  and  $r_0(\text{Fe}^{\text{II}}-\text{O}) = 1.734$  Å,  $r_0(\text{Co}^{\text{II}}-\text{F}) = 1.649$  and  $r_0(\text{Co}^{\text{II}}-\text{O}) = 1.692$  Å.<sup>27,28</sup>



**Figure 6.** Views of the O,F disorder in the single crystal structure (a), and theoretical O,F ordering in model 1 (b), model 2 (c), and model 3 (d).

Starting from the disordered structure of Fe(OH)F, one may build at least three different ordered models. Since there are only two positions for the fluorine atoms (F1 and F2), we considered in the ordered model 1 that F<sup>-</sup> and OH<sup>-</sup> occupy the sites 1 and 2, respectively. This induces the formation of a *bent* hydrogen bond with a F1...H2-O2 angle of 146.2 ° (Figure 6b). Inspection of databases  
5 surprisingly revealed that a such hydrogen bond does not occur in any of the ordered oxyhydroxide MOOH or hydroxyfluoride M(OH)F compounds; however it does occur in Sr(OH)<sub>2</sub> (*Pnma*,  $a = 9.8890$ ,  $b = 3.9184$ ,  $c = 6.1202$  Å,  $V = 237.15$  Å<sup>3</sup>, and O1...H2-O2 angle = 146.79 °) (Figure 6c).<sup>29</sup> It is worth noting that although Sr(OH)<sub>2</sub> has been intensively studied, since all the investigators used a coordination number of 7 for Sr<sup>2+</sup>, they could not see the strong structural relationship with the  
10 ramsdellite and the diaspore structures. When we use a coordination number of 6 for Sr<sup>2+</sup>, this relationship becomes obvious (Figure 6c, e).

In model 2, we considered that F<sup>-</sup> and OH<sup>-</sup> occupy the sites 2 and 1, respectively. The resulting structure is isostructural to the diaspore-type (Figure 6d, e). Most of the oxyhydroxide compounds crystallise with this type of structure. However, there are large differences in the geometry of the *bent*  
15 hydrogen bond among these compounds. In Fe(OH)F, the F2...H1-O1 angle is 173.39 °, while the O-H...H angles are 171.41, 160.89, and 152.36 ° in α-MnOOH, α-AlOOH, and α-GaOOH, respectively.<sup>4, 12, 30</sup>

In Model 3, we attempted to alternate F<sup>-</sup> and OH<sup>-</sup> along the tunnels. Several steps were required to achieve this. The *Pnma* symmetry was first lowered to *P1*, then the *b* cell parameter was doubled ( $a =$   
20  $10.471$ ,  $b = 6.4118$ ,  $c = 4.6977$  Å), the OH<sup>-</sup> and F<sup>-</sup> anions ordered one by one, and finally the 32 atomic positions determined (Figure 6d). Finally, using the Platon suite of crystallographic programs,<sup>31</sup> we determined that a higher symmetry cell exists with the *P2<sub>1</sub>/c* space group, with parameters  $a = 6.4118$ ,  $b = 4.6977$ ,  $c = 10.471$  Å, and  $\beta = 90$  °,  $Z = 8$ , and 8 new atomic positions (Figure 6f).

The crystal structure of Co(OH)<sub>0.86(3)</sub>F<sub>1.14(3)</sub> is very similar to that of Fe(OH)F. Interatomic distances

and BVSS<sup>27, 28</sup> are listed in Table 4. The  $\text{Co}(\text{O},\text{F})_6$  octahedra are regular in shape. The  $\text{Co}-(\text{O},\text{F})$  distances range from 2.073 to 2.093 Å with an average value of 2.083 Å slightly lower than the average value 2.1 Å estimated from the sum of the ionic radius of  $\text{Co}^{2+}$  (0.745 Å),  $\text{F}^-$  (1.31 Å) and  $\text{O}^{2-}$  (1.4 Å).<sup>32</sup> In  $\text{Co}(\text{OH})_{0.86(3)}\text{F}_{1.14(3)}$ , *bent* hydrogen bonds occur with  $\text{O2-H2}\dots\text{F1}$  and  $\text{O1-H1}\dots\text{F2}$  angles of 163.37 and 150.01 °, respectively.

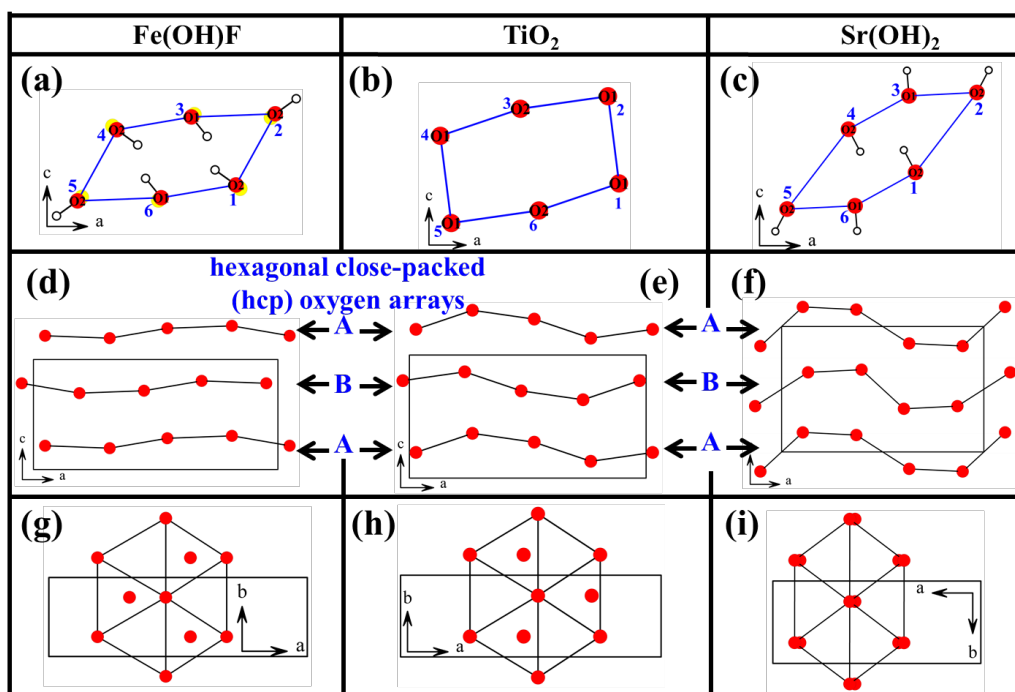


**Figure 7.** Distortion of the hexagonal close packed oxygen arrays in  $\text{Fe}(\text{OH})\text{F}$ , ramsdellite-type- $\text{TiO}_2$ , and  $\text{Sr}(\text{OH})_2$ .

10 Our three theoretical ordered models of  $\text{Fe}(\text{OH})\text{F}$  may also be observed for the stoichiometric  $\text{Co}(\text{OH})\text{F}$  compound. Among these three models, the probability of occurrence for model 3 appears to be much higher than for models 1 or 2, since protons have been experimentally observed at distances from O1 and O2 between 0.85 and 1.00 Å. In models 1 and 2, the protons are attached only to O1 or O2.

15 Careful examination of different compounds with structures related to the ramsdellite-type (Table 5)



revealed few differences. Indeed, the *hcp* oxygen arrays are only slightly distorted in Fe(OH)F and Co(OH)F, whereas in ramsdellite-type-TiO<sub>2</sub> and especially in Sr(OH)<sub>2</sub>, they are strongly distorted (Figure 7d-i). Such distortions induce the formation of tunnels with different shapes (*i.e.*, parallelogram, rectangle, elongated hexagon in Fe(OH)F, TiO<sub>2</sub> and Sr(OH)<sub>2</sub>, respectively) (Figure 7a-  
5 c).

**Table 5.** Compounds with a crystal structure related to the diaspore and ramsdellite-type structure.

Compounds	<i>a</i> (Å)	<i>c</i> (Å)	<i>b</i> (Å)	Ref.
diaspore $\alpha$ -AlO(OH)	9.4210	2.8450	4.4010	4
$\alpha$ -GaO(OH)	9.7907	2.9732	4.5171	30
Groutite $\alpha$ -MnO(OH)	10.6670	2.8710	4.5540	12
Groutellite (MnO <sub>1.5</sub> (OH) <sub>0.5</sub> )	9.5155	2.8644	4.706	2
$\alpha$ -ScO(OH)	10.3010	3.2090	4.7550	33
Bracewellite CrO(OH)	9.860	2.974	4.492	34
Montroseite VO(OH)	9.97	3.03	4.54	35
Goethite $\alpha$ -FeO(OH)	9.956	3.0215	4.608	36
CoO(OH) HP	9.402	2.840	4.353	37
$\alpha$ -GaO(OD)	9.779	2.966	4.516	38
MgF(OH)	10.116	3.0794	4.6888	15
ZnF(OH)	10.228	3.1125	4.765	21
CoF(OH)	10.305	3.126	4.677	16
FeF(OH)	10.471	3.2059	4.6977	*
Ramsdellite MnO <sub>2</sub>	9.27	2.866	4.533	39
Ramsdellite TiO <sub>2</sub>	9.459	2.9585	4.9022	40
VO <sub>2</sub>	9.39	2.93	4.89	41
CNb <sub>2</sub>	10.76	3.135	4.966	42
IrTe <sub>2</sub>	13.5116	4.0671	5.5275	43
Sr(OH) <sub>2</sub>	9.8890	3.9184	6.1202	29

\* : from this work

### 3.3. Co(OH)F magnetic properties

10 The results of magnetic property measurements for Co(OH)F are presented in Figure 8. The molar magnetic susceptibility  $\chi_m$  as a function of temperature revealed a signature of a magnetic transition at  $T \sim 40$  K. Above  $\sim 150$  K the corresponding  $1/\chi_m$  curve follows the Curie-Weiss law. A linear fit in the range 200–300 K yielded  $\Theta = -61.4$  K and an effective moment  $5.39 \mu_B$ , indicating predominantly  
antiferromagnetic interactions in the system, with a substantial contribution from the unquenched  
15 orbital moment in addition to the spin-only value for d<sup>7</sup> Co<sup>2+</sup>.

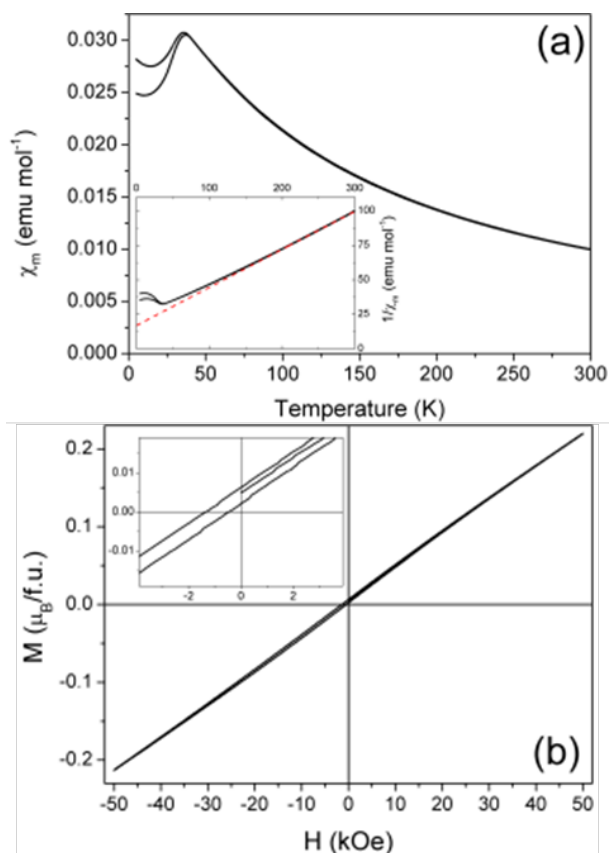


**Figure 8.** (a) Molar magnetic susceptibility  $\chi_m$  of  $\text{Co(OH)}_{0.86(3)}\text{F}_{1.14(3)}$  as a function of temperature. The inset shows the corresponding  $1/\chi_m$  and the linear fit with the Curie-Weiss function (red dashed line). (b) Magnetisation  $M$  as a function of field  $H$  for a 50 kOe field-cooled sample at 5 K.

5

We attribute the observed ZFC/FC curve divergence at  $T_N$  and weak ferromagnetic hysteresis at 2 K (Figure 8a) to the uncompensated moments from structural defects and on the particle surfaces (so called superantiferromagnetism)<sup>44</sup> which can reasonably be expected for hydrothermally produced  $\text{Co(OH)F}$ . The phenomenon is well known in antiferromagnetic goethite  $\text{FeOOH}$ <sup>45</sup> and ferritin with antiferromagnetic cores of  $\text{FeOOH}\cdot x\text{H}_2\text{O}$ .<sup>46</sup> Magnetically, the bulk of such materials develop long-range order while the surface demonstrates spin-glass behaviour<sup>47</sup>. The latter results in a characteristic frequency dependence of the magnetic susceptibility, which was indeed confirmed in the present case by AC susceptibility measurements (Figure S4).

The shift of the hysteresis loop for the field cooled (5 T) sample (Figure 8b) also points to the

presence of uncompensated spins on particle surfaces resulting in an exchange-biased AFM/FM core-shell structure.<sup>48</sup> This has previously been observed in hydrothermally prepared goethite.<sup>49</sup> The similarity between the bulk magnetic structure of CoOHF and that of goethite FeOOH is discussed further below.

### 3.4. Co(OH)F magnetic structure from neutron powder diffraction measurements

Examination of the neutron diffraction patterns collected at 3 K and 75 K revealed additional diffraction peaks, presumably due to magnetic ordering. This is consistent with the magnetic susceptibility data which suggested an antiferromagnetic transition at ~40 K (Figure 8). All the diffraction peaks of  $\text{Co(OH)}_{0.86(3)}\text{F}_{1.14(3)}$  with magnetic contribution could be indexed by the crystallographic unit cell, *i.e.*, with the propagation vector  $k = (0,0,0)$ . For the  $4c(x, 0.25, z)$  Wyckoff site of the  $Pnma$  space group the magnetic representation decomposes in terms of eight one-dimensional irreducible representations (IR) as  $\Gamma = \Gamma_1 + 2\Gamma_2 + 2\Gamma_3 + \Gamma_4 + \Gamma_5 + 2\Gamma_6 + 2\Gamma_7 + \Gamma_8$ . The associated basis vectors are listed in Table S1.† The best agreement between the experimental and calculated powder diffraction patterns was obtained for the  $\Gamma_4$  representation (equivalent to the  $Pnma'$  Shubnikov group, Opechowski-Guccione number 62.445). The magnetic structure of  $\text{Co(OH)}_{0.86(3)}\text{F}_{1.14(3)}$  can be described as antiferromagnetic ordering of ferromagnetic rutile-type chains of trans-edge sharing octahedra with the moments parallel to the short  $b$ -axis (Figure 9). It is qualitatively the same as that originally reported for goethite  $\alpha$ -FeOOH,<sup>50</sup> which is not surprising as strong interchain superexchange dominates in the case of  $d^7$   $\text{Co}^{2+}$  the same way it does for the  $d^5$   $\text{Fe}^{3+}$  analogue as expected from the Goodenough-Kanamori rules.<sup>51</sup> Since one of the later studies of magnetic structure of goethite suggested possible spin canting along the longest  $a$ -axis<sup>52</sup>, we carefully tested the presence of such a magnetic mode but found no evidence of non-collinearity. We also note that an additional antiferromagnetic mode allowing spin canting along the  $a$ -axis would require mixing of basis vectors  $A_y$  and  $G_x$  of two irreducible representations (Table S1)† and lowering the magnetic

symmetry to  $P2_1'2_1'2_1$  which is unlikely given there is no evidence that the magnetic transition in goethite is not second-order. Therefore, we concluded that our NPD data for  $\text{Co}(\text{OH})_{0.86(3)}\text{F}_{1.14(3)}$  supports the collinear model  $Pnma'$ . The final Rietveld plot and the crystallographic information for the 3 K NPD data are presented in Figure S3 and Table S2,<sup>†</sup> respectively. The moment value determined for  $\text{Co}(\text{OH})_{0.86(3)}\text{F}_{1.14(3)}$  from the NPD data collected at 3 K,  $2.41(3) \mu_B$ , is significantly lower than the theoretical value for high-spin  $d^7 \text{Co}^{2+}$ , especially taking into account some contribution from an unquenched orbital moment, most likely due to chemical disorder of F and OH locally distorting Co-X-Co magnetic exchange paths (Table 4).

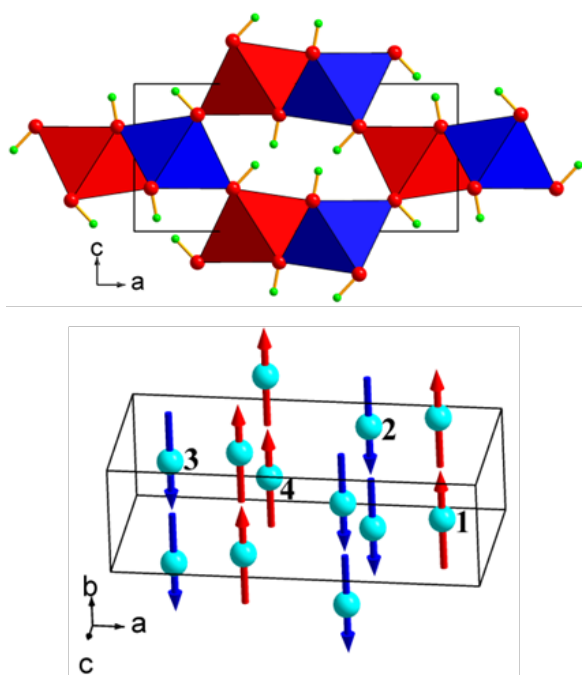


**Figure 9.** Magnetic structure of  $\text{Co}(\text{OH})_{0.86(3)}\text{F}_{1.14(3)}$  at 3 K. Top: the red and blue octahedra show cobalt sites with spins up and down, respectively; bottom: same with diamagnetic atoms omitted for clarity.

## Conclusions

The new compounds Fe(OH)F and Co(OH)<sub>0.86(3)</sub>F<sub>1.14(3)</sub> synthesized by a hydrothermal route were obtained serendipitously during the preparation of the new phase LiMOF ( $M = \text{Fe}$  and  $\text{Co}$ ). These compounds crystallize with distorted ramsdellite-type structures related to the well-known diaspore  $\alpha$ -AlOOH-type. The structures consist of double chains of edge-sharing  $M(\text{F},\text{O})_6$  octahedra running along the  $b$ -axis. These infinite chains share corners, giving rise to infinite channels. Protons are located in the channels and form O-H...F bent hydrogen bonds. Magnetic susceptibility data for Co(OH)<sub>0.86(3)</sub>F<sub>1.14(3)</sub> indicate antiferromagnetic ordering below  $\sim 40$  K and neutron powder diffraction measurements at 3 K show that ferromagnetic rutile-type chains with spins parallel to the  $b$ -axis are antiferromagnetically coupled to each other, similarly to the magnetic structure of goethite  $\alpha$ -FeOOH.

10

## Acknowledgments

This work was financially supported by Grant-in-Aid for Japan Society for the Promotion of Science (JSPS) Fellows Grant Number 24•02506 and the Australian Research Council (DP110102662).

15

## References

- (1) Kondrashev, Y.D.; Zaslavskii, A.I. *Izv. Akad. Nauk SSSR (Ser. Fiz.)* **1951**, *15*, 179.
- (2) Post, J.E.; Heaney, P.J. *Am. Mineral.* **2004**, *89*, 969.
- (3) Legrand, C.; Delville, J. *C. R. Hebd. Seances Acad. Sci.* **1953**, *236*, 944.
- 20 (4) Busing, W.R.; Levy, H.A. *Acta Crystallogr.* **1958**, *11*, 798.
- (5) Haines, J.; Léger, J.M.; Hoyau, S. *J. Phys. Chem. Solids* **1995**, *56*, 965.
- (6) Rossouw, M.H.; Liles, D.C.; Thackeray, M.M.; David, W.I.F.; Hull, S. *Mater. Res. Bull.* **1992**, *27*, 221

- (7) Hunter, J.C. *J. Solid State Chem.* **1981**, 39,142.
- (8) Kijima, N.; Takahashi, Y.; Akimoto, J.; Awaka, J. *J. Solid State Chem.* **2005**,178, 2741.
- (9) Ling, C.; Mizuno, F. *Chem. Mater.* **2012**, 24, 3943.
- (10) Du, G.; Wang, J.; Guo, Z.; Chen, Z.; Liu, H. *Mater. Lett.* **2011**, 65, 1319.
- 5 (11) Rogulski, Z.; Chotkowski, M.; Czerwinski, A. *J. New Mater. Electrochem. Syst.* **2006**, 9, 401.
- (12) Kohler, T.; Armbruster, T.; Libowitzky, E. *J. Solid State Chem.* **1997**, 133, 486.
- (13) Christensen, A.N.; Ollivier, G. *Solid State Commun.* **1972**, 10, 609.
- (14) Feitknecht, V.M.; Brunner, P.; Oswald, H.R. *Z. Anorg. Allgem. Chem.* **1962**, 316, 154.
- (15) Crichton, W. A.; Parise, J. B.; Müller, H.; Breger, J.; Marshall, W. G.; Welch, M. D. *Mineral.*  
10 *Mag.* **2012**, 76, 25.
- (16) Rodriguez, M.A.; Millan, P.; Rojas, R.M.; Garcia, O. *J. Therm. Anal.* **1995**, 44, 395.
- (17) Lange, B.A.; Haendler, H.M. *J. Inorg. Nucl. Chem.* **1973**, 35, 3129.
- (18) Scholz, G.; Stosiek, C.; Feist, M.; Kemnitz, E. *Eur. J. Inorg. Chem.* **2012**, 14, 2337.
- (19) Peter, S.; Weckler, B.; Roisnel, T.; Lutz, H. D. *Bull. Chem. Technol. Macedonia* **1997**, 16, 21.
- 15 (20) Giester, G.; Libowitzky, E. *Z. Kristallogr.* **2003**, 218, 351.
- (21) Serier, H.; Gaudon, M.; Demourgues, A.; Tressaud, A. *J. Solid State Chem.* **2007**, 180, 3485.
- (22) Stalhandske, C. *Acta Crystallogr.* **1979**, B35, 2184.
- (23) Ben Yahia, H.; Shikano, M.; Kobayashi, H.; Avdeev, M.; Liu, S.; Ling, C.D. *Phys. Chem.*  
*Chem. Phys.* **2013**, 15, 13061.
- 20 (24) Petricek, V.; Dusek, M.; Palatinus, L. (2006). *Jana2006. The crystallographic computing system*. Institute of Physics, Praha, Czech Republic.
- (25) Okudera, H.; Kihara, K.; Matsumoto, T. *Acta Crystallogr.* **1996**, B52, 450.
- (26) Rodriguez-Carvajal, J. *Phys. B* **1993**, 192, 55.
- (27) Brown, I. D.; Altermatt, D. *Acta Crystallogr.* **1985**, B41, 244.
- 25 (28) Brese, N. E.; O'Keefe, M. *Acta Crystallogr.* **1991**, B47, 192.

- (29) Giese, R.F. Jr. *Z. Kristallogr.* **1977**, *146*, 205.
- (30) Li, S.J.; Zheng, C.; Lobring, K.C. *Z. Kristallogr.* **2003**, *218*, 11.
- (31) Spek, A. L. PLATON, A Multipurpose Crystallographic Tool, Utrecht University, Utrecht, The Netherlands, **2008**.
- 5 (32) Shannon, R. D. *Acta Crystallogr., Sect. A: Cryst. Phys., Diffr., Theor. Gen. Crystallogr.* **1976**, *A32*, 751.
- (33) Christensen, A.N.; Jensen, S.J. *Acta Chem. Scand.* **1967**, *21*, 121.
- (34) Fleischer, M.; Cabri, L.J.; Nickel, E.H.; Pabst, A. *Am. Mineral.* **1977**, *62*, 593400.
- (35) Evans, H.T.; Mrose, M.E. U.S. geological survey Washington 25, D.C.
- 10 (36) Sampson, C. F. *Acta Cryst.* **1969**, *B25*, 1683.
- (37) Chevanas, J.; Joubert, J.C.; Capponl, J.J. *J. Solid State Chem.* **1973**, *6*, 1.
- (38) Pye, M.F.; Birtill, J.J.; Dickens, P.G. *Acta Crystallogr.* **1977**, *B33*, 3224.
- (39) Byström, A.M. *Acta Chem. Scand.* **1949**, *3*, 163.
- (40) Akimoto, J.; Gotoh, Y.; Oosawa, Y.; Nonose, N.; Kumagai, T.; Aoki, K.; Takei, H. *J. Solid*  
15 *State Chem.* **1994**, *113*, 27.
- (41) Evans, H.T. Jr.; Mrose, M.E. *Am. Mineral.* **1955**, *40*, 861.
- (42) Alyamovskii, S.I.; Shveikin, G.P.; Gei, P.V. *Russ. J. Inorg. Chem.* **1963**, *8*, 1042.
- (43) Jobic, S.; Brec, R.; Pasturel, A.; Koo, H.J.; Whangbo, M.H. *J. Solid State Chem.* **2001**, *162*, 63.
- (44) Néel, L. *C. R. Acad. Sci.* **1962**, *252*, 4075.
- 20 (45) Liu, Q.; Torrent, J.; Yu, Y.; Deng, C. *J. Geophys. Res.* **2004**, *109*, B12106.
- (46) Gilles, C.; Bonville, P.; Rakoto, H.; Broto, J.M.; Wong, K.K.W.; Mann, S. *J. Magn. Magn. Mater.* **2002**, *241*, 430.
- (47) Laguta, V. V., Glinchuk, M. D., Marysko, M., Kuzian, R. O., Prosandeev, S. A., Raevskaya, S. I., Smotrakov, V. G., Eremkin, V. V., Raevski, I. P. *Phys. Rev. B.* **2013**, *87*, 064403.

- (48) Nogués, J.; Sort, J. ; Langlais, V. ; Skumryev, V. ; Surinach, S. ; Munoz, J. S. ; Baró., M. D.  
*Physics Reports* **2005**, *422 no. 3*, 65.
- (49) Barrero, C. A.; Betancur, J. D.; Greneche, J. M.; Goya, G. F.; Berquó, T. S. *Geophys. J. Int.*  
**2006**, *164*, 331.
- 5 (50) Forsyth, J. B.; Hedley, I. G.; Johnson., C. E. *J. Phys.* **1968**, *C1*, 179.
- (51) Goodenough, J. B. *Phys. Rev.*, **1955**, *100*, 564; J. Kanamori, *J. Phys. Chem. Solids* **1959**, *10*,  
87.
- (52) Coey, J.M.D.; Barry, A.; Brotto, J.; Rakoto, H.; Brennan, S.; Mussel, W. N.; Collomb, A.;  
Fruchart., D. *J. Phys. Condens. Mat.* **1995**, *7 no. 4*, 759.
- 10 (53) Krezhov, K.; Petrov, K.; Karamaneva, T. *J. Solid State Chem.* **1983**, *48*, 33.



## Table of contents caption and figure

The title compounds crystallize with structures related to the diaspore-type  $\alpha$ -AlOOH. The protons are located in the channels and form O-H...F *bent* hydrogen bonds. The magnetic susceptibility data for cobalt phase indicate antiferromagnetic ordering below  $\sim 40$  K and the neutron powder diffraction measurements at 3 K show that ferromagnetic rutile-type chains with spins parallel to the *b*-axis are antiferromagnetically coupled to each other, similarly to the magnetic structure of goethite  $\alpha$ -FeOOH.

